


Optical transport lengths quantifying depolarization in experiments on random media

Maximilian Gill ¹, Bruno Gompf ^{1,*}, Martin Dressel ¹ and Gabriel Schnoering ^{1,2,†}

¹*Physikalisches Institut, Universität Stuttgart, Pfaffenwaldring 57, 70569 Stuttgart, Germany*

²*Laboratory of Thermodynamics in Emerging Technologies, ETH Zurich, Sonneggstrasse 3, Zurich, Switzerland*

 (Received 9 November 2021; revised 25 February 2022; accepted 18 March 2022; published 13 May 2022)

When light diffuses in random media, the intensity decays and at the same time the polarization state is scrambled. As explanation for this apparent inseparability, theoretical work has identified a profound relation between length scales of optical transport and depolarization. Here, we experimentally confirm and quantify their proportionality with thickness-dependent depolarization measurements in colloidal suspensions of microscopic constituents. The observed equivalences accurately predict the nonlinear evolution rate of depolarization over a large range of penetration depths. Our results provide a simple relation, that connects light diffusion in strongly scattering media with measurable polarization signatures over wide spectral ranges and scatterer concentrations.

DOI: [10.1103/PhysRevA.105.053511](https://doi.org/10.1103/PhysRevA.105.053511)

I. INTRODUCTION

In many research fields, from astronomy, atmospheric physics, and spectroscopy down to bio-imaging, multiple scattering progressively changes the direction and original polarization state of light [1–6]. The transformations of these two seemingly independent properties of light are correlated to each other in structurally random media [7,8]. In these media, the diffusion of light is governed by two length scales, the mean free path ℓ describing the interspace between two scattering events and the transport mean free path ℓ^* corresponding to the distance that light travels until its direction \mathbf{k} is randomized, as illustrated in Fig. 1(a) [9]. Efforts to clarify their relationship to depolarization promise to supply numerous optical fields of study with new analytical tools. Randomization of the propagation direction of light is common in interstellar dust [10], clouds [11], biological tissues [12,13], turbid media [14], and in general in all “white” matter. In observations, randomization of the polarization state manifests as depolarization. Depolarization is a macroscopic observable that arises from ensemble averaging of polarized fields over intervals of time or space smaller than that of the acquisition. Despite its stochastic nature, the measurement of depolarization enables the recovery of microscopic parameters and processes that are difficult to observe by other means [9]. Examples are refractive indices in inhomogeneous media or distances between microscopic defects and their motion [7–9].

The present paper demonstrates that dynamic light transport quantities ℓ and ℓ^* can be directly obtained from depolarization measurements. Our paper provides an experimental confirmation that these quantities are equivalent to length scales of depolarization and quantifies their proportionality. Previously, studies on Rayleigh and Mie scatterers have suggested the connection between length scales of optical depolarization and diffusion of light [7]. More recently, corresponding explicit expressions have been theoretically established in [15,16]. They are valid for the diffusive regime for which polarization resolved optical transport equations were derived in [17,18]. To analyze the dynamics of polarized light transport we, however, draw on a phenomenological model that is especially suited for experimental data. We measure light depolarization as a function of the light penetration depth into media through Mueller matrix ellipsometry [19–23]. We then describe the evolution of polarization states with a random-walk model [24,25] that naturally gives rise to measurable depolarization length scales. Finally, we compare their values and spectra to predictions for ℓ and ℓ^* .

II. EXPERIMENTAL SETUP

Uniform colloidal suspensions are prepared at various volume fractions ϕ between 0.5 and 9.6% by mixing pure water with a commercial master solution (microparticles.de) of $\phi = 9.6\%$. The suspension consists of polystyrene spheres of diameter $1.5 \pm 0.05 \mu\text{m}$. Interparticle correlations and their influence on ℓ and ℓ^* are negligible at these concentrations [26]. The particle density (1.05 g/cm^3) is similar to that of water and no sedimentation was observed over the duration of experiments.

For measurements, the suspensions are injected via a syringe into a commercial fluid cell (Omni Cell, Specac), the thickness $z = 12\text{--}2000 \mu\text{m}$ of which is adjusted by a variety of Polytetrafluoroethylene (PTFE) spacers. To fully determine

*b.gompf@pi.uni-stuttgart.de

†schngabr@ethz.ch

Published by the American Physical Society under the terms of the [Creative Commons Attribution 4.0 International license](https://creativecommons.org/licenses/by/4.0/). Further distribution of this work must maintain attribution to the author(s) and the published article's title, journal citation, and DOI.

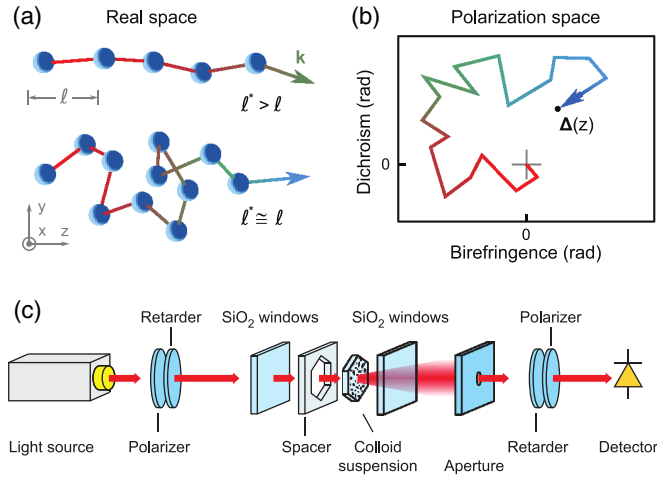


FIG. 1. (a) Sketch of the randomization of \mathbf{k} in real space for two different ratios of ℓ^*/ℓ . A shorter transport mean free path ℓ^* implies faster randomization. (b) A random walk of the optical property Δ in the birefringence or dichroism plane represents the randomization of polarization [see Eq. (3)]. (c) Schematic of the experiment. Polarized and collimated LED light is sent through a colloidal suspension of fixed size spheres over varying thicknesses. The outgoing light is analyzed with polarization optics and a photodiode and the resulting Mueller matrix is obtained

their optical response the z -dependent Mueller matrices are acquired in the visible and near infrared from 385 to 940 nm at normal incidence and room temperature with a Woollam VASE ellipsometer equipped with additional compensators to acquire all 16 Mueller matrix elements. In an ellipsometer the sample is illuminated by a collimated beam with various well-defined polarization states, and, after interaction with the sample, the polarization changes are analyzed. The Mueller matrix, obtained in this way, contains the entire polarization response of our samples for a given thickness and particle concentration. As is detailed below, our experimental conditions are such that only the diagonal terms are significant; they directly give, after decomposition, the depolarizations σ_b^2 for the different polarization bases [22].

To provide sufficient optical intensity, high power LEDs with low coherence are employed as light sources and with spectral bandwidths of $\Delta\lambda \sim 10$ nm to avoid speckles. The incident beam is collimated to ensure a pure polarization state \mathbf{S}_{in} and has a diameter of 5 mm while the emerging diffuse beam is detected through a 5-mm aperture. Reproducibility is successfully verified by repetitively measuring specific data points (λ, ϕ) on different days and samples. A schematic of the setup is shown in Fig. 1(c).

The Brownian motion of the particles influences the experimental Mueller matrices on time scales of $t_{\text{acq}} \sim 0.1$ s, which is much smaller than the measurement time $t_{\text{acq}} \sim 30$ s. As a consequence, the detector captures a large ensemble of light paths. However, we stress that, instead of being detrimental to the results, this effect ensures better statistics due to the consideration of a larger ensemble of particle configurations. In the analysis, this is taken into account by the averaging operator $\langle \dots \rangle$ as discussed in Eq. (2) of the main text.

III. RESULTS AND DISCUSSION

A. Polarized light diffusion in random media

Stochastic modeling approaches successfully reproduce polarization signatures caused by multiple scattering in experiments on random media [7,24,25]. Early observations showed a linear evolution of depolarization quantities at large light penetration depths z that agreed well with Monte Carlo simulations [7]. Later studies put forth analytical stochastic differential equations for polarization diffusion that showed a more accurate correspondence with measured depolarization values and provided a deeper picture about contributing phenomena [25]. The depolarization curve as a function of z displays two regimes: a linear evolution at large z and a nonlinear transient behavior at short z . Each regime exhibits distinct polarization dynamics [25], that are discussed in more detail in the following.

Using ℓ and ℓ^* in a random medium, light propagation can be modeled as an ensemble of photon trajectories. Each photon with position $\mathbf{r}(t)$ performs an isotropic random walk with direction changes due to stochastic scattering processes. Its mean-squared displacement $\sigma_r^2(\tau) = \langle |\mathbf{r}(t + \tau) - \mathbf{r}(t)|^2 \rangle$ follows the equation [27]

$$\sigma_r^2(\tau) = D\tau \quad (1)$$

over a time duration τ , where D is the diffusion coefficient defined by $D = c\ell^*/3$, c is the energy velocity of light in the medium, and $\langle \dots \rangle$ denotes ensemble averaging.

Since the dynamics in real space are governed by characteristic length scales, we expect the same to be true in polarization space. In analogy to the coordinate vector of light \mathbf{r} in real space, a set of three two-dimensional vectors Δ_b , ($b \in \{L, L45, C\}$) encodes the accumulated polarization state of the light in the birefringence-dichroism space [Fig. 1(b)]. These elements exist in three different bases—linear (L), linear at $\pm 45^\circ$ ($L45$), and circular (C) [28]—and change randomly at each scattering event. The mean-squared polarization displacement,

$$\sigma_b^2(z) = \langle |\Delta_b(z) - \Delta_b(0)|^2 \rangle, \quad (2)$$

defines the depolarization and depends on the light penetration depth z into the medium [24,25]. In analogy to Eq. (1), experiments have shown that $\sigma_b^2(z)$ satisfies [7,25]

$$\lim_{z \gg z_b^T} \sigma_b^2(z) = B_b z + K_b, \quad (3)$$

for large z , with z_b^T a characteristic length scale that is defined below. Comparison of Eqs. (1) and (3) reveals that B_b defines a diffusion coefficient for polarization states and its inverse B_b^{-1} is the associated depolarization length scale. The additional variance K_b accounts for depolarization contributions earlier along the z propagation. It is a testimony to the fact that the polarization diffusion $\sigma_b^2(z)$ exhibits different statistics at small penetration depths $0 \leq z \lesssim z_b^T$ when compared to $\sigma_r^2(t)$. These contributions are short lived and decay exponentially over the *transient regime* z_b^T [25]. Previous studies found that $\sigma_b^2(z)$ evolves nonlinearly in this regime [23,25]. This behavior quickly recedes as z enters the *stationary regime* for $z \geq z_b^T$. The two length scales z_b^T and B_b^{-1} are prominent

features of depolarization and summarize the overall behavior of different $\sigma_b^2(z)$ curves.

In order to determine z_b^T and B_b^{-1} experimentally, the depolarization curve $\sigma_b^2(z)$ needs to be acquired in both characteristic regimes. The random perturbation of $\Delta_b(z)$ along the propagation direction z follows an Ornstein-Uhlenbeck process [29], i.e., a stochastic differential equation, the coefficients of which encode microscopic dynamics. The accumulated optical property relates to its *polarization velocity* $\mathbf{p}_b(z)$ through

$$\Delta_b(z) = \int_0^z \mathbf{p}_b(s) ds. \quad (4)$$

$\mathbf{p}_b(z)$ satisfies the stochastic differential equation [30]:

$$\frac{d\mathbf{p}_b(z)}{dz} = \mathbf{A}_b \mathbf{p}_b(z) + \Sigma_b \frac{d\mathbf{N}_b(z)}{dz}, \quad (5)$$

with $\mathbf{N}_b(z)$ a unit normal noise vector, Σ_b a real 2×2 noise amplitude, and \mathbf{A}_b a real 2×2 drift matrix.

As a consequence, the dynamics of $\mathbf{p}_b(z)$ are not completely random, but originate from an interplay between random noise provided by $\mathbf{N}_b(z)$ and deterministic interchange and damping given by \mathbf{A}_b [Eq. (5)]. At short distances z , the term $\mathbf{A}_b \mathbf{p}_b(z)$ dominates. At large distances both terms drive the dynamics. For this reason the depolarization $\sigma_b^2(z)$ experiences two distinct regimes at different scales of z [Eq. (3)].

The analytic expression for the z -dependent curves of $\sigma_b^2(z)$, derived from Eqs. (2), (4), and (5) (see Appendices), is later fitted to the experimental data. The fits provide estimates for the coefficients \mathbf{A}_b and Σ_b , that define explicit expressions for $B_b^{-1} = B_b^{-1}(\mathbf{A}_b, \Sigma_b)$ and $z_b^T = z_b^T(\mathbf{A}_b)$. The present paper correlates these coefficients to the physical properties of the individual scatterers in random media. To do so effectively, we perform experiments on a model system with microscopic scatterers, the optical properties of which are well defined.

B. Light depolarization measurements

In our experiments we measure $\Delta_b(z)$ and its uncertainties $\sigma_b^2(z)$ by Mueller matrix ellipsometry [20] and subsequent differential decomposition of the matrices [21–23]. We do this for uniform colloidal suspensions of spherical polystyrene (PS) particles with diameter $2r = 1.5 \mu\text{m}$ at different volume fractions ϕ and a wide range of sample thicknesses z illuminated in transmission by low-coherence sources at various wavelengths λ . Volume fractions as large as 9.6% are probed which still allow neglecting optical short-range interactions [31–33]. Together with the refractive indices of the scatterers n_p and solvent n_s our system is then fully characterized.

The spherical symmetry of the scatterers reduces the system description to only three variables (x, m, ϕ) , with the size parameter $x = \frac{2\pi n_s r}{\lambda}$ and the relative refractive index $m = \frac{n_p}{n_s}$ [34]. A change in the wavelength λ is equivalent to an inverse change in the particle radius r . Consequently, our results can be extended to (λ, r, n_s, n_p) that lead to similar (x, m) .

Colloidal suspensions of PS spheres have several advantages [26]. They are easy to control experimentally and their single-particle scattering is described exactly through Mie theory, from which the length scales ℓ and ℓ^* are computed as functions of (x, ϕ, m) [9]. Any change in these variables will lead to different evolution of $\mathbf{p}_b(z)$. Due to their symmetry, the scatterers depolarize exclusively by multiple scattering. The closeness of the density of water and PS spheres suppresses sedimentation over the course of the experiment. The thermodynamic behavior of the beads is also well understood. We make use of known relationships between ϕ and the structure factor during the computation of (ℓ, ℓ^*) to account for interparticle correlations [35,36]. Furthermore, polystyrene spheres of $1.5 \mu\text{m}$ exhibit minuscule optical absorption and a large scattering cross section in the visible spectrum.

Large single-particle scattering cross sections are crucial in order to access both depolarization regimes (transient and stationary) experimentally. The strongly increasing attenuation due to multiple scattering as a function of z constrains the available z range. Particle sizes with the largest scattering cross sections maximize the therein generated depolarization.

C. Relation between light depolarization lengths and transport parameters

We want to express light depolarization in terms of the transport parameters ℓ and ℓ^* . Therefore, it is important to differentiate their signatures in spectra of z_b^T and B_b^{-1} . This is possible for the chosen size of PS beads because ℓ and ℓ^* exhibit distinct spectral behaviors. While the mean free path ℓ displays a minimum at 600 nm, due to a Mie resonance, the transport mean free path ℓ^* increases monotonically with the wavelength as presented in Fig. 2(a).

Our suspensions of $1.5\text{-}\mu\text{m}$ PS spheres generate noise that matches the Gaussian process described by Eqs. (4) and (5). All measured Mueller matrices are diagonal, i.e., they are perfect depolarizers and produce maximum entropy [37,38]. For this reason, an incident Stokes vector $\mathbf{S}^{\text{in}} = (S_0^{\text{in}}, S_1^{\text{in}}, S_2^{\text{in}}, S_3^{\text{in}})^T$ produces the outgoing Stokes vector $\mathbf{S}^{\text{out}}(z)$ that reads [25]

$$\mathbf{S}^{\text{out}}(z) = I(z) \begin{pmatrix} S_0^{\text{in}} \\ S_1^{\text{in}} \exp[-\sigma_{L45}^2(z) - \sigma_C^2(z)] \\ S_2^{\text{in}} \exp[-\sigma_L^2(z) - \sigma_C^2(z)] \\ S_3^{\text{in}} \exp[-\sigma_L^2(z) - \sigma_{L45}^2(z)] \end{pmatrix}, \quad (6)$$

with the transmitted irradiance $I(z)$, the Stokes parameters S_{0-3} , and the depolarizations σ_b^2 [Eq. (2)] associated with polarization bases $b \in \{L, L45, C\}$. The mean values $\langle \Delta_b(z) \rangle$ vanish and do not contribute in Eq. (6) because the Mueller matrices are diagonal. We assume that the nonzero variances $\sigma_b^2(z)$ are predominant compared to higher-order statistical moments, as is confirmed in the following, where we demonstrate the accuracy of the model.

Good agreement is observed between measurements and fits of $\sigma_b^2(z)$ as shown in Fig. 2(b) for the three optical properties L , $L45$, and C , at chosen $(\phi = 1.1\%, \lambda = 530 \text{ nm})$. The stochastic model perfectly reproduces the expected transient and stationary regimes of the data. Over the transient regime, $0 \lesssim z < z_b^T$, the variance $\sigma_b^2(z)$ evolves nonlinearly,

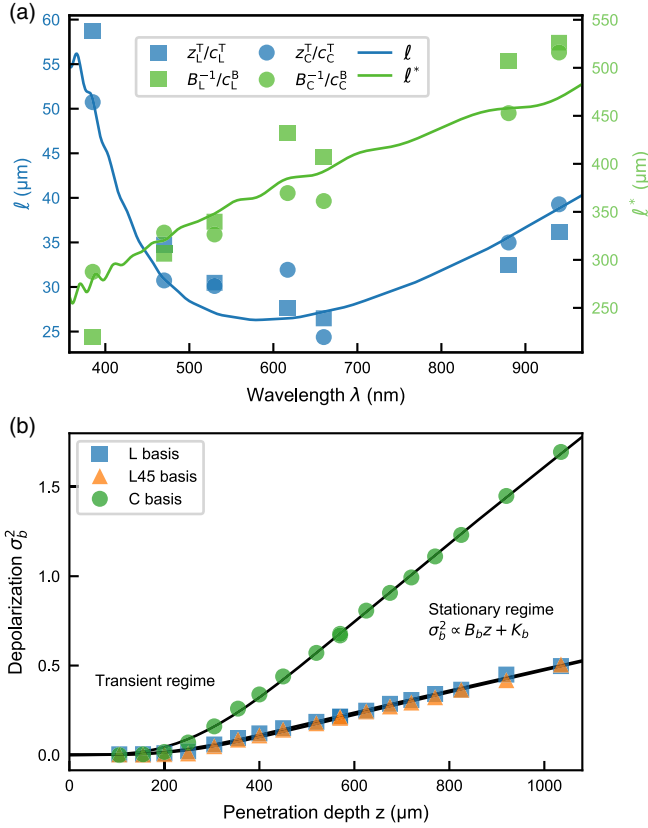


FIG. 2. (a) Light transport quantities (solid lines) ℓ in blue (dark gray) and ℓ^* in green (light gray) show distinct spectra. Measured depolarization length scales z_b^T in blue (dark gray) symbols and B_b^{-1} in green (light gray) symbols follow ℓ and ℓ^* for linear (square) and circular (circle) polarization [Eq. (7)]. (b) Measured depolarization (symbols) with corresponding fits to Eq. (5) (solid lines) as a function of sample thickness z for a wavelength $\lambda = 530$ nm. Each data set belongs to one of the bases, linear L (square), linear $L45$ (triangle), and circular C (circle). The transient regime is characterized by z_b^T . The diffusion coefficient B_b gives rise to the linear growth of depolarization in the stationary regime. Its inverse B_b^{-1} is the corresponding depolarization length. All graphs are drawn at a volume fraction of $\phi = 1.1\%$ and sphere size $2r = 1.5$ μm .

and subsequently enters the stationary regime, $z_b^T < z$, where it approaches the linear trend of Eq. (3). Excellent correspondence between data and model is observed for all measured (λ, ϕ) .

We experimentally varied the wavelength over $\lambda \in [385 \text{ nm}; 940 \text{ nm}]$ and recovered the spectra of z_b^T and B_b^{-1} as shown in Fig. 2(a). Here, clear differences between the two quantities are seen. While z_b^T exhibits a minimum around $\lambda = 600$ nm, B_b^{-1} increases monotonically with λ for all polarization bases. They follow ℓ and ℓ^* , the spectra of which are overlaid with associated colors. This relationship persists when the volume fraction $\phi \in [0.48\%; 9.6\%]$ is varied. It is also observed that all length scales decrease monotonically with increasing ϕ .

To investigate the apparent relationship between these length scales, in Fig. 3 all measured data for z_b^T and B_b^{-1} are plotted as functions of ℓ and ℓ^* , respectively. All points follow

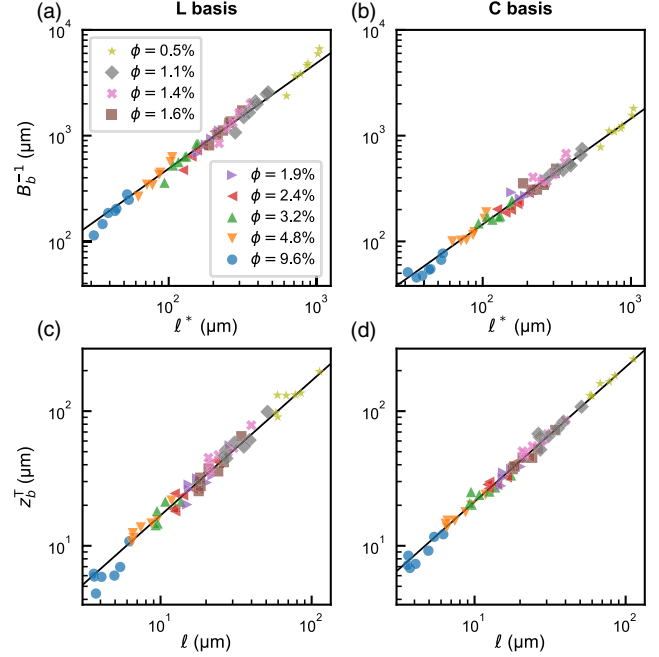


FIG. 3. Depolarization length B_b^{-1} (a, b) and transient length z_b^T (c, d) plotted as functions of ℓ^* and ℓ , respectively. Data points were obtained from parameters \mathbf{A}_b and $\mathbf{\Sigma}_b$ using fits to Eq. (5), while ℓ and ℓ^* were computed from Mie theory using the known values of (ϕ, x) . Each color and symbol corresponds to a different volume fraction of scatterers measured at different wavelengths. The left and right columns correspond to linear (L) and circular (C) polarization, respectively.

straight lines evidencing a simple proportionality between the length scales. Hence, we obtain the following relationships:

$$\begin{aligned} z_b^T(\ell) &= c_b^T \ell(\lambda, \phi), \\ B_b^{-1}(\ell^*) &= c_b^B \ell^*(\lambda, \phi), \end{aligned} \quad (7)$$

with fitted dimensionless coefficients c_b^T and c_b^B reported in Table I. The direct proportionality holds over nearly two orders of magnitude with no additional contributions.

This result directly links depolarization to the properties of the scattering medium. Explicit formulas are well established for (ℓ, ℓ^*) [9]. By substitution into Eq. (7) they generate explicit formulas for (z_b^T, B_b^{-1}) in terms of the medium properties (x, ϕ) . This not only enables quantitative predictions of depolarization, but also offers new avenues to measure (ℓ, ℓ^*) . Polarization measurements allow us to determine ℓ and ℓ^* using Eqs. (4)–(7). This provides the advantage that acquisition times much longer than the fast diffusion of light

TABLE I. Linearity coefficients (c_b^T , c_b^B) between real and polarization spaces as given by Eq. (7), fit from Fig. 3 and given with 95% confidence intervals (linear L , linear $L45$, and circular C).

	L	$L45$	C
c_b^T	1.68 ± 0.05	1.70 ± 0.06	2.13 ± 0.04
c_b^B	4.88 ± 0.14	4.85 ± 0.13	1.45 ± 0.04

are sufficient. The following discussion highlights the wide validity of the coefficients c_b^T and c_b^B for random media.

We expect that the values of c_b^T and c_b^B are not only invariant with respect to λ and ϕ but also to r for a suspension of spheres and fixed illumination conditions. In our experiments the parameters (x, ϕ, m) fully characterize length scales for multiple scattering [9,34] and depolarization. The wavelength and particle radius contribute equally in the ratio x and do not occur elsewhere. Consequently, a change of wavelength λ is equivalent to an inverse change of radius r and results in the same x and (ℓ, ℓ^*) . Therefore, the observed invariance of the coefficients (c_b^T, c_b^B) with respect to x includes λ and r .

With Eq. (7) there is experimental evidence for a deep physical connection between the randomization of the propagation direction of light \mathbf{k} and depolarization. Our results indicate that, in random media, it is impossible to restrict diffusion to only the polarization or the real space. Both domains appear inseparable and the coefficients (c_b^T, c_b^B) give measures for how the rates of their dynamics compare to each other. For example, c_L^T gives a transient regime z_L^T lasting ≈ 1.7 scattering events (Table I). After this distance the depolarization dynamics approach their long-term steady-state behavior. Here, with a factor of $c_L^B \approx 4.9$, the rate $1/\ell^*$ at which the \mathbf{k} vector is disoriented is considerably higher than the rate of depolarization B_L . Diffusion of circularly polarized light through the medium is slower compared to linearly polarized light, because c_C^B is smaller than c_L^B and c_{L45}^B .

Finally, the experimental result in Eq. (7) reveals details about the physical processes behind the depolarization dynamics. It establishes the following relationship between the drift matrix \mathbf{A}_b and ℓ upon substitution of $z_b^T(\mathbf{A}_b) = 1/\sqrt{\det(\mathbf{A}_b)}$:

$$\det(\mathbf{A}_b) = (c_b^T \ell)^{-2}. \quad (8)$$

This has conceptual implications. In the phenomenological model [Eq. (5)] the drift matrix \mathbf{A}_b encodes the deterministic dynamics that connect past and present values of $\mathbf{p}(z)$. Its inverse determinant quantifies the resilience of the polarization during diffusion in the medium. Therefore, a small determinant protects the state from perturbations over long distances. Experimentally, Eq. (8) shows that ℓ characterizes the deterministic processes. These dominate the dynamics at the beginning of the medium and cause the nonlinear evolution of $\sigma_b^2(z)$ in the transient regime $0 \leq z \leq z_b^T$. We expect that the relationship of ℓ and \mathbf{A} stems from the deterministic nature of single scattering, where changes in polarization amount to linear maps.

In similar fashion, the model Eq. (5) endows B_b^{-1} with a mixed dependence on \mathbf{A} and Σ . Given the experimental link between \mathbf{A} and ℓ in Eq. (8), it is natural to ask whether B_b^{-1} is also a function of ℓ . This idea is supported by theory given in [16] where depolarization lengths are presented as simultaneous functions of ℓ and ℓ^* . Despite this, we were unable to observe any such effect under our experimental conditions. In the diffusion regime ($z \gg z^T$), the associated depolarization length scale B^{-1} depends on ℓ^* only [Eq. (7)]. Contributions from \mathbf{A} and Σ associated with ℓ are absent.

IV. CONCLUSION

In conclusion, we present an experimental confirmation of recent theoretical work that connects length scales associated with light transport with those related to depolarization in random media [16]. Here, we observe direct proportionality for both ℓ and ℓ^* and their respective depolarization length scales in the transient and stationary regimes. These optical relations hold for wide ranges of particle density and wavelength. We anticipate that the presented relations between simple-to-calculate parameters ℓ and ℓ^* and depolarization metrics z_b^T and B_b^{-1} will greatly aid efforts to optically determine the distances between scatterers through polarization measurements.

ACKNOWLEDGMENTS

The work was supported by the Deutsche Forschungsgemeinschaft via Grant No. DR228/38-1. We are thankful to Kevin Vynck and Romain Pierrat for discussions on the theoretical relation between optical transport length scales and related depolarization length scales. G.S. thanks Thibault Chervy for helpful discussions.

APPENDIX A: MEAN FREE PATHS

In ensembles of spherical scatterers the mean free paths ℓ and ℓ^* depend on individual and collective properties of the particles [9]:

$$\begin{aligned} \ell &= \left(\frac{3\phi}{2k_s^2 r^3} \int_0^{2k_s} \frac{dC_{\text{sca}}}{dq} F(q, \phi) q dq \right)^{-1}, \\ \ell^* &= \left(\frac{3\phi}{4k_s^4 r^3} \int_0^{2k_s} \frac{dC_{\text{sca}}}{dq} F(q, \phi) q^3 dq \right)^{-1}. \end{aligned} \quad (A1)$$

Here, k_s is the \mathbf{k} vector inside the solvent, r the radius of the spheres, and ϕ their volume fraction. The integration is performed numerically. The differential scattering cross section $dC_{\text{sca}}/d\Omega$ follows from Mie theory and is given by the series [34]

$$\frac{dC_{\text{sca}}}{d\Omega} = \frac{2\pi}{k_s^2} \left| \sum_{l=0}^{\infty} \sqrt{2l+1} (a_l \mathbf{X}_{l,\pm 1} \pm ib_l \hat{\mathbf{r}} \times \mathbf{X}_{l,\pm 1}) \right|^2, \quad (A2)$$

which converges sufficiently around the order

$$l_{\text{max}} = \text{floor}(k_s r + 4.05(k_s r)^{1/3} + 2). \quad (A3)$$

We use the following definition for the vector spherical harmonics [35],

$$\mathbf{X}_{l,m} = \frac{\widehat{\mathbf{L}} Y_{l,m}(\theta, \phi)}{\sqrt{l(l+1)}}, \quad (A4)$$

in terms of the standard spherical harmonics $Y_{l,m}$ and angular momentum operator $\widehat{\mathbf{L}}$. The coefficients a_l and b_l read

$$a_l = \frac{j_l(kr) \frac{d}{du} [u j_l(k_s u)]_{u=r} - \frac{k_p}{k_s} \frac{\mu_p}{\mu_s} j_l(k_p r) \frac{d}{du} [u j_l(k_s u)]_{u=r}}{\frac{k_p}{k_s} \frac{\mu_p}{\mu_s} j_l(k_p r) \frac{d}{du} [u h_l^{(1)}(k_s u)]_{u=r} - h_l^{(1)}(k_s r) \frac{d}{du} [u j_l(k_p u)]_{u=r}},$$

$$b_l = \frac{\frac{\mu_p}{\mu_s} j_l(k_s r) \frac{d}{du} [u j_l(k_s u)]_{u=r} - \frac{k_p}{k_s} j_l(k_p r) \frac{d}{du} [u j_l(k_s u)]_{u=r}}{\frac{k_p}{k_s} j_l(k_p r) \frac{d}{du} [u h_l^{(1)}(k_s u)]_{u=r} - \frac{\mu_p}{\mu_s} h_l^{(1)}(k_s r) \frac{d}{du} [u j_l(k_p u)]_{u=r}}, \quad (\text{A5})$$

with $j_l(x)$ the spherical Bessel functions and $h_l^{(1)}(x)$ spherical Hankel functions of the first kind. Here μ is the magnetic permeability and the subscripts “p” and “s” denote quantities inside the particle and the solvent, respectively.

The mean free paths ℓ and ℓ^* [Eq. (A1)] use the Percus-Yevick approximation [36] for the static structure factor of hard spheres given by

$$F(q, \phi) = \frac{1}{1 - \overline{NC}(q, \phi)}, \quad (\text{A6})$$

where

$$\begin{aligned} \overline{NC}(q, \phi) = & -24\phi \left(\lambda_1 \left[\frac{\sin(2qr) - (2qr) \cos(2qr)}{(2qr)^3} \right] \right. \\ & - 6\phi \lambda_2 \left[\frac{[(2qr)^2 - 2] \cos(2qr) - 2(2qr) \sin(2qr) + 2}{(2qr)^4} \right] \\ & \left. - \phi \frac{\lambda_1}{2(2qr)^6} \{ [(2qr)^4 - 12(2qr)^2 + 24] \cos(2qr) + [24(2qr) - 4(2qr)^3] \sin(2qr) - 24 \} \right). \end{aligned} \quad (\text{A7})$$

This expression depends on the volume fraction ϕ , the spheres radius r , and the parameters λ_1 and λ_2 which are defined as

$$\lambda_1 = \frac{(1 + 2\phi)^2}{(1 - \phi)^4} \quad \text{and} \quad \lambda_2 = \frac{-(1 + \phi/2)^2}{(1 - \phi)^4}. \quad (\text{A8})$$

The structure factor $F(q, \phi)$ is based on the statistical mechanics of hard sphere colloids and characterizes their spatial correlations. Within our experimental ranges for wavelengths λ and volume fractions ϕ , contribution from the structure factor $F(q, \phi)$ only weakly perturbs the behavior of ℓ and ℓ^* .

APPENDIX B: EXPRESSION FOR DEPOLARIZATION

The two-element vector $\Delta_b(z)$ describes polarization changes in the birefringence-dichroism space in one of the three possible polarization bases $b \in \{L, L45, C\}$. The rate $\mathbf{p}_b(z) = \frac{d}{dz} \Delta_b(z)$ satisfies the stochastic differential equation given by

$$\frac{d\mathbf{p}_b(z)}{dz} = \mathbf{A}_b \mathbf{p}_b(z) + \Sigma_b \frac{d\mathbf{N}_b(z)}{dz}, \quad (\text{B1})$$

and has the formal solution [25]

$$\mathbf{p}_b(z) = e^{\mathbf{A}_b z} \mathbf{p}_b(z_0) + \int_{z_0}^z e^{\mathbf{A}_b(z-r)} \Sigma_b d\mathbf{N}(r). \quad (\text{B2})$$

Our system of colloidal spheres does not polarize at $z = 0$. Therefore, we set

$$\Delta_b(z_0) = \mathbf{p}_b(z_0) = 0, \quad \text{and} \quad z_0 = 0. \quad (\text{B3})$$

Through the use of Itô's isometry [25] we obtain the covariance matrix of \mathbf{p}_b

$$\begin{aligned} \text{Cov}[\mathbf{p}_b(u), \mathbf{p}_b(v)] &= \langle \mathbf{p}_b(u) \mathbf{p}_b^T(v) \rangle \\ &= \int_0^{\min(u,v)} e^{\mathbf{A}_b(u-r)} \Sigma_b \Sigma_b^T e^{\mathbf{A}_b^T(v-r)} dr \end{aligned} \quad (\text{B4})$$

and the covariance matrix of Δ_b :

$$\begin{aligned} \text{Cov}[\Delta_b(s), \Delta_b(t)] &= \\ &\times \int_0^s du \int_0^t dv \int_0^{\min(u,v)} e^{\mathbf{A}_b(u-r)} \Sigma_b \Sigma_b^T e^{\mathbf{A}_b^T(v-r)} dr. \end{aligned} \quad (\text{B5})$$

The experimentally accessible depolarization $\sigma_b^2(z)$ is the trace of Eq. (B5) evaluated at $s = t = z$, which permits the following simplifications:

$$\begin{aligned} \sigma_b^2(z) &= \text{Tr} \left\{ \int_0^z du \int_0^z dv \int_0^{\min(u,v)} e^{\mathbf{A}_b(u-r)} \Sigma_b \Sigma_b^T e^{\mathbf{A}_b^T(v-r)} dr \right\} \\ &= \int_0^z du \int_0^z dv \int_0^{\min(u,v)} \text{Tr} \{ e^{\mathbf{A}_b(u-r)} \mathbf{R}^T \mathbf{Q}_b \mathbf{R} e^{\mathbf{A}_b^T(v-r)} \} dr \\ &= \iiint \text{Tr} \{ \mathbf{R}^T e^{\Gamma_b(u-r)} \mathbf{R} \mathbf{R}^T \mathbf{Q}_b \mathbf{R} e^{\Gamma_b^T(v-r)} \mathbf{R} \} dudvdr \\ &= \int_0^z du \int_0^z dv \int_0^{\min(u,v)} \text{Tr} \{ e^{\Gamma_b(u-r)} \mathbf{Q}_b e^{\Gamma_b^T(v-r)} \} dr. \end{aligned} \quad (\text{B6})$$

The product $\Sigma_b \Sigma_b^T$ is symmetric and positive semidefinite which allows its diagonalization by a rotation matrix $\mathbf{R}(\beta)$ with angle β and $\mathbf{Q}_b = \text{diag}[q_{b,1}^2, q_{b,2}^2]$. To eliminate \mathbf{R} , we first transform \mathbf{A}_b into a new matrix $\Gamma_b = \mathbf{R} \mathbf{A}_b \mathbf{R}^T$. Then we use the trace invariance with respect to cyclic permutations of factors and the identity $\mathbf{R} \mathbf{R}^T = \mathbb{1}$. This simplification is desirable because it reduces the parameter space to six independent variables ($\Gamma_{b,11}, \Gamma_{b,12}, \Gamma_{b,21}, \Gamma_{b,22}, q_{b,1}^2, q_{b,2}^2$). Note

that the rotation angle β does not appear in the final expression of Eq. (B6). The 2×2 matrices $\mathbf{\Gamma}_b$ and \mathbf{Q}_b are determined through fits. Although the drift matrix \mathbf{A}_b can not be fully recovered, its properties such as its determinant and trace are shared by $\mathbf{\Gamma}_b$. The two matrices are related through an unknown similarity transformation $\mathbf{\Gamma}_b = \mathbf{R}\mathbf{A}_b\mathbf{R}^T$.

The rotational invariance of the expression for $\sigma_b^2(z)$ with respect to $\mathbf{R}(\beta)$ implies that the six recovered parameters in general describe the evolution of $\mathbf{p}_b(z)$ in coordinates that are arbitrarily rotated with respect to birefringence-

dichroism coordinates. Out of the eight degrees of freedom given by the parameters of \mathbf{A}_b and $\mathbf{\Sigma}_b$ the experimentally observed evolution for $\sigma_b^2(z)$ has two that are not directly measurable.

Initial fits showed that the eigenvalues of \mathbf{A}_b are always complex conjugates. In the following this is used to further simplify the expression of Eq. (B6) with the introduction of the real $\gamma_b/2$ and imaginary $\omega_b/2$ parts of the eigenvalues of \mathbf{A}_b . The six parameters of the model then read $(\gamma_b, \omega_b, \mathbf{\Gamma}_{b,12}, \mathbf{\Gamma}_{b,21}, q_{b,1}^2, q_{b,2}^2)$. With

$$\begin{aligned}\gamma_b &= \text{Tr}(\mathbf{A}_b) = \mathbf{A}_{b,11} + \mathbf{A}_{b,22} = 2\text{Re}[\text{eig}(\mathbf{A}_b)], \\ \omega_b &= i\sqrt{(\mathbf{A}_{b,11} - \mathbf{A}_{b,22})^2 + 4\mathbf{A}_{b,12}\mathbf{A}_{b,21}} = 2\text{Im}[\text{eig}(\mathbf{A}_b)],\end{aligned}\quad (\text{B7})$$

and after integration of Eq. (B6), the model of $\sigma_b^2(z)$ has the following general form:

$$\begin{aligned}\sigma_b^2(z) &= B_b z + K_b + [D_b \cos(\omega_b z/2) + E_b \sin(\omega_b z/2)]e^{\gamma_b z/2} \\ &\quad + [G_b \cos(\omega_b z) + H_b \sin(\omega_b z) + I_b]e^{\gamma_b z}.\end{aligned}\quad (\text{B8})$$

The coefficients have the following explicit expressions:

$$\begin{aligned}B_b &= \frac{-2}{(\gamma_b^2 + \omega_b^2)^2} [(q_{b,1}^2 + q_{b,2}^2)(\omega_b^2 - \gamma_b^2) - 4(\mathbf{\Gamma}_{b,12} - \mathbf{\Gamma}_{b,21})(\mathbf{\Gamma}_{b,12}q_{b,2}^2 - \mathbf{\Gamma}_{b,21}q_{b,1}^2) \\ &\quad + 2\gamma_b(q_{b,1}^2 - q_{b,2}^2)(-\omega_b^2 - 4\mathbf{\Gamma}_{b,12}\mathbf{\Gamma}_{b,21})^{\frac{1}{2}}],\end{aligned}\quad (\text{B9})$$

$$\begin{aligned}K_b &= \frac{1}{\gamma_b(\gamma_b^2 + \omega_b^2)^3} [6(q_{b,1}^2 + q_{b,2}^2)(\gamma_b^2 - 3\omega_b^2)\gamma_b^2 + 4(11\gamma_b^2 - \omega_b^2)(\mathbf{\Gamma}_{b,12} - \mathbf{\Gamma}_{b,21})(\mathbf{\Gamma}_{b,12}q_{b,2}^2 - \mathbf{\Gamma}_{b,21}q_{b,1}^2) \\ &\quad - 6(q_{b,1}^2 - q_{b,2}^2)\gamma_b(3\gamma_b^2 - \omega_b^2)(-\omega_b^2 - 4\mathbf{\Gamma}_{b,12}\mathbf{\Gamma}_{b,21})^{\frac{1}{2}}],\end{aligned}\quad (\text{B10})$$

$$\begin{aligned}D_b &= \frac{-1}{(\gamma_b^2 + \omega_b^2)^3} [(8\gamma_b^3 - 24\gamma_b\omega_b^2)(q_{b,1}^2 + q_{b,2}^2) + (q_{b,2}^2 - q_{b,1}^2)(24\gamma_b^2 - 8\omega_b^2)(-\omega_b^2 - 4\mathbf{\Gamma}_{b,12}\mathbf{\Gamma}_{b,21})^{\frac{1}{2}} \\ &\quad + 64\gamma_b(\mathbf{\Gamma}_{b,12} - \mathbf{\Gamma}_{b,21})(\mathbf{\Gamma}_{b,12}q_{b,2}^2 - \mathbf{\Gamma}_{b,21}q_{b,1}^2)],\end{aligned}\quad (\text{B11})$$

$$\begin{aligned}E_b &= \frac{1}{\omega_b(\gamma_b^2 + \omega_b^2)^3} [(8\omega_b^4 - 24\gamma_b^2\omega_b^2)(q_{b,1}^2 + q_{b,2}^2) + 32(\mathbf{\Gamma}_{b,12} - \mathbf{\Gamma}_{b,21})(-\mathbf{\Gamma}_{b,21}q_{b,1}^2 + \mathbf{\Gamma}_{b,12}q_{b,2}^2)(\gamma_b^2 - \omega_b^2) \\ &\quad + (24\gamma_b\omega_b^2 - 8\gamma_b^3)(q_{b,1}^2 - q_{b,2}^2)(-\omega_b^2 - 4\mathbf{\Gamma}_{b,12}\mathbf{\Gamma}_{b,21})^{\frac{1}{2}}],\end{aligned}\quad (\text{B12})$$

$$\begin{aligned}G_b &= \frac{1}{\omega_b^2(\gamma_b^2 + \omega_b^2)^3} [(q_{b,1}^2 - q_{b,2}^2)(2\omega_b^4 - 6\gamma_b^2\omega_b^2)(-\omega_b^2 - 4\mathbf{\Gamma}_{b,12}\mathbf{\Gamma}_{b,21})^{\frac{1}{2}} + (2\gamma_b^3\omega_b^2 - 6\gamma_b\omega_b^4)(q_{b,1}^2 + q_{b,2}^2) \\ &\quad + (12\gamma_b\omega_b^2 - 4\gamma_b^3)(\mathbf{\Gamma}_{b,12} - \mathbf{\Gamma}_{b,21})(\mathbf{\Gamma}_{b,12}q_{b,2}^2 - \mathbf{\Gamma}_{b,21}q_{b,1}^2)],\end{aligned}\quad (\text{B13})$$

$$\begin{aligned}H_b &= \frac{-1}{\omega_b(\gamma_b^2 + \omega_b^2)^3} [(2\omega_b^4 - 6\gamma_b^2\omega_b^2)(q_{b,1}^2 + q_{b,2}^2) + (12\gamma_b^2 - 4\omega_b^2)(\mathbf{\Gamma}_{b,12} - \mathbf{\Gamma}_{b,21})(\mathbf{\Gamma}_{b,12}q_{b,2}^2 - \mathbf{\Gamma}_{b,21}q_{b,1}^2) \\ &\quad + (6\gamma_b\omega_b^2 - 2\gamma_b^3)(q_{b,1}^2 - q_{b,2}^2)(-\omega_b^2 - 4\mathbf{\Gamma}_{b,12}\mathbf{\Gamma}_{b,21})^{\frac{1}{2}}],\end{aligned}\quad (\text{B14})$$

$$I_b = \frac{4}{\gamma_b\omega_b^2(\gamma_b^2 + \omega_b^2)} (\mathbf{\Gamma}_{b,12} - \mathbf{\Gamma}_{b,21})(\mathbf{\Gamma}_{b,12}q_{b,2}^2 - \mathbf{\Gamma}_{b,21}q_{b,1}^2).\quad (\text{B15})$$

We define the depolarization length scales as follows. From Eq. (B8) it is evident that all terms except $B_b z + K_b$ decay exponentially when $\gamma < 0$ for large penetration depths z . This condition is satisfied throughout our data and leads

to the expression

$$\lim_{z \gg 0} \sigma_b^2(z) = B_b z + K_b, \quad (\text{B16})$$

and the identification of B_b^{-1} as the stationary depolarization length [Eq. (B9)]. The eigenvalues of \mathbf{A}_b [Eq. (B7)] define the rate of decay for the nonlinear terms in Eq. (B8). Hence, the length of the transient regime is proportional to $z_b^\top(\mathbf{A}_b) = 1/\sqrt{\det(\mathbf{A}_b)} = 2/\sqrt{\gamma^2 + \omega^2}$.

Note that $\sigma_b^2(z)$ of Eq. (B8) is positive semidefinite for $z > 0$ due to its derivation from the covariance matrix in Eq. (B5). Therefore, the depolarization curve automatically passes through the origin. With Eq. (B16) this implies that B_b is strictly positive. Propagation in the stationary regime can only increase, not decrease depolarization.

-
- [1] J. Hough, Polarimetry: A powerful diagnostic tool in astronomy, *Astronomy and Geophysics* **47**, 3.31 (2006).
- [2] K. Akiyama, J. C. Algaba, A. Alberdi, W. Alef, R. Anantua, K. Asada, R. Azulay, A.-K. Baczko, D. Ball, M. Baloković *et al.*, First M87 event horizon telescope results. VII. Polarization of the ring, *Astrophys. J. Lett.* **910**, L12 (2021).
- [3] C. M. Sorensen, Light scattering by fractal aggregates: A review, *Aerosol Sci. Technol.* **35**, 648 (2001).
- [4] M. C. Roggemann and B. M. Welsh, *Imaging Through Turbulence* (CRC, Boca Raton, FL, 2018).
- [5] V. Ntziachristos, Going deeper than microscopy: the optical imaging frontier in biology, *Nature Methods* **7**, 603 (2010).
- [6] N. Ghosh and A. I. Vitkin, Tissue polarimetry: concepts, challenges, applications, and outlook, *J Biomed. Opt.* **16**, 110801 (2011).
- [7] D. Bicout, C. Brosseau, A. S. Martinez, and J. M. Schmitt, Depolarization of multiply scattered waves by spherical diffusers: Influence of the size parameter, *Phys. Rev. E* **49**, 1767 (1994).
- [8] C. Brosseau and D. Bicout, Entropy production in multiple scattering of light by a spatially random medium, *Phys. Rev. E* **50**, 4997 (1994).
- [9] L. F. Rojas-Ochoa, S. Romer, F. Scheffold, and P. Schurtenberger, Diffusing wave spectroscopy and small-angle neutron scattering from concentrated colloidal suspensions, *Phys. Rev. E* **65**, 051403 (2002).
- [10] J. Weingartner and B. Draine, Dust grain-size distributions and extinction in the milky way, large magellanic cloud, and small magellanic cloud, *Astrophys. J.* **548**, 296 (2001).
- [11] J. E. Hansen, Multiple scattering of polarized light in planetary atmospheres part ii. sunlight reflected by terrestrial water clouds, *J. Atmos. Sci.* **28**, 1400 (1971).
- [12] A. E. Profio, Light transport in tissue, *Appl. Opt.* **28**, 2216 (1989).
- [13] T. Liu, T. Sun, H. He, S. Liu, Y. Dong, J. Wu, and H. Ma, Comparative study of the imaging contrasts of Mueller matrix derived parameters between transmission and backscattering polarimetry, *Biomedical Optics Express* **9**, 4413 (2018).
- [14] D. A. Weitz, J. X. Zhu, D. J. Durian, H. Gang, and D. J. Pine, Diffusing-wave spectroscopy: The technique and some applications, *Phys. Scr.* **T49B**, 610 (1993).
- [15] K. Vynck, R. Pierrat, and R. Carminati, Polarization and spatial coherence of electromagnetic waves in uncorrelated disordered media, *Phys. Rev. A* **89**, 013842 (2014).
- [16] K. Vynck, R. Pierrat, and R. Carminati, Multiple scattering of polarized light in disordered media exhibiting short-range structural correlations, *Phys. Rev. A* **94**, 033851 (2016).
- [17] E. Akkermans and G. Montambaux, *Mesoscopic Physics of Electrons and Photons* (Cambridge University, New York, 2007).
- [18] R. Carminati and J. C. Schotland, *Principles of Scattering and Transport of Light* (Cambridge University, New York, 2021).
- [19] N. Ortega-Quijano and J. L. Arce-Diego, Mueller matrix differential decomposition, *Opt. Lett.* **36**, 1942 (2011).
- [20] H. Fujiwara, *Spectroscopic Ellipsometry: Principles and Applications* (Wiley, New York, 2007).
- [21] R. M. A. Azzam, Propagation of partially polarized light through anisotropic media with or without depolarization: A differential 4×4 matrix calculus, *J. Opt. Soc. Am.* **68**, 1756 (1978).
- [22] R. Ossikovski, Differential matrix formalism for depolarizing anisotropic media, *Opt. Lett.* **36**, 2330 (2011).
- [23] N. Agarwal, J. Yoon, E. Garcia-Caurel, T. Novikova, J.-C. Vanel, A. Pierangelo, A. Bykov, A. Popov, I. Meglinski, and R. Ossikovski, Spatial evolution of depolarization in homogeneous turbid media within the differential Mueller matrix formalism, *Opt. Lett.* **40**, 5634 (2015).
- [24] V. Devlaminck, Depolarizing differential Mueller matrix of homogeneous media under gaussian fluctuation hypothesis, *J. Opt. Soc. Am. A* **32**, 1736 (2015).
- [25] J. M. Charbois and V. Devlaminck, Stochastic model for the differential Mueller matrix of stationary and nonstationary turbid media, *J. Opt. Soc. Am. A* **33**, 2414 (2016).
- [26] G. L. Hunter and E. R. Weeks, The physics of the colloidal glass transition, *Rep. Prog. Phys.* **75**, 066501 (2012).
- [27] R. Pierrat, J.-J. Greffet, and R. Carminati, Photon diffusion coefficient in scattering and absorbing media, *J. Opt. Soc. Am. A* **23**, 1106 (2006).
- [28] R. C. Jones, A new calculus for the treatment of optical systems vii properties of the n-matrices, *J. Opt. Soc. Am.* **38**, 671 (1948).
- [29] G. E. Uhlenbeck and L. S. Ornstein, On the theory of the Brownian motion, *Phys. Rev.* **36**, 823 (1930).
- [30] B. Øksendal, *Stochastic Differential Equations: An Introduction with Applications* (Springer-Verlag, Berlin, 1998).
- [31] S. Fraden and G. Maret, Multiple Light Scattering from Concentrated, Interacting Suspensions, *Phys. Rev. Lett.* **65**, 512 (1990).
- [32] P. M. Saulnier, M. P. Zinkin, and G. H. Watson, Scatterer correlation effects on photon transport in dense random media, *Phys. Rev. B* **42**, 2621 (1990).
- [33] L. F. Rojas-Ochoa, J. M. Mendez-Alcaraz, J. J. Sáenz, P. Schurtenberger, and F. Scheffold, Photonic Properties of Strongly Correlated Colloidal Liquids, *Phys. Rev. Lett.* **93**, 073903 (2004).

- [34] C. F. Bohren and D. R. Huffman, *Absorption and scattering of light by small particles* (John Wiley & Sons, 2008).
- [35] J. D. Jackson, *Classical electrodynamics*, 3rd ed. (Wiley, New York, NY, 1998).
- [36] M. S. Wertheim, Exact Solution of the Percus-Yevick Integral Equation for Hard Spheres, [Phys. Rev. Lett. **10**, 321 \(1963\)](#).
- [37] G. Puentes, D. Voigt, A. Aiello, and J. P. Woerdman, Experimental observation of universality in depolarized light scattering, [Opt. Lett. **30**, 3216 \(2005\)](#).
- [38] A. Aiello and J. P. Woerdman, Physical Bounds to the Entropy-Depolarization Relation in Random Light Scattering, [Phys. Rev. Lett. **94**, 090406 \(2005\)](#).